Energy budget-based backscatter in a shallow water model of a double gyre basin

Milan Klöwer, Malte Jansen, Martin Claus, Richard J Greatbatch, Soeren Thomsen

▶ To cite this version:

HAL Id: hal-02053501

https://hal.sorbonne-universite.fr/hal-02053501v1

Submitted on 1 Mar 2019

Accepted Manuscript

Energy budget-based backscatter in a shallow water model of a double gyre basin

Milan Klöwer, Malte F. Jansen, Martin Claus, Richard J. Greatbatch, Sören Thomsen
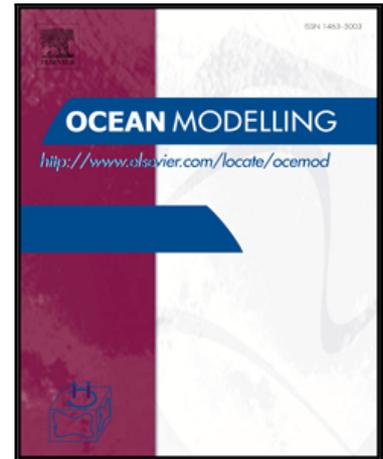
Please cite this article as: Milan Klöwer, Malte F. Jansen, Martin Claus, Richard J. Greatbatch, Sören Thomsen, Energy budget-based backscatter in a shallow water model of a double gyre basin, *Ocean Modelling* (2018), doi: https://doi.org/10.1016/j.ocemod.2018.09.006

Highlights

- Generalization of the energy budget backscatter for a sub-grid eddy parameterization

- Rossby number-dependent dissipation scaling controls the forward energy-cascade

- Parameterization is tested successfully in a double gyre basin shallow water model

- The energy cycle of the model is considerably improved at low computational cost

1

Energy budget-based backscatter in a shallow water model of a double gyre basin

Milan Klöwer[a,b,*], Malte F. Jansen[c], Martin Claus[a,d],
Richard J. Greatbatch[a,d], Sören Thomsen[a,e]

[a]*GEOMAR Helmholtz Centre for Ocean Research Kiel, Kiel 24105, Germany*
[b]*Atmospheric, Oceanic and Planetary Physics, University of Oxford, Oxford OX1 3PU, UK*
[c]*Department of the Geophysical Sciences, University of Chicago, Chicago, IL 60637, USA*
[d]*Faculty of Mathematics and Natural Sciences, University of Kiel, Kiel 24118, Germany*
[e]*LOCEAN-IPSL, IRD/CNRS/Sorbonne University (UPMC)/MNHN, Paris 75252, France*

Abstract

The parameterization of sub-grid scale processes is one of the key challenges towards improved numerical simulations of the atmospheric and oceanic circulation. Numerical weather prediction models as well as climate models would benefit from more sophisticated turbulence closures that allow for less spurious dissipation at the grid-scale and consequently higher and more realistic levels of eddy kinetic energy (EKE). Recent studies propose to use a hyperviscous closure in combination with an additional deterministic forcing term as a negative viscosity to represent backscatter of energy from unresolved scales. The sub-grid EKE is introduced as an additional prognostic variable that is fed by dissipation at the grid scale, and enables recycling of EKE via the backscatter term at larger scales. This parameterization was previously shown to work well in zonally re-entrant channel configurations. Here, a generalization in the form of a Rossby number-dependent scaling for the strength of the backscatter is introduced to represent the emergence of a forward energy-cascade in unbalanced flows near the boundaries. We apply the parameterization to a shallow water model of a double gyre basin and provide evidence for its general applicability. In terms of mean state and variability, a low resolution model is considerably

---

*Corresponding author
Email address:* `milan.kloewer@physics.ox.ac.uk` (Milan Klöwer)

improved towards a high resolution control run at low additional computational cost.

1. Introduction

Mesoscale eddies are a key turbulent feature of the global oceans (Chelton et al., 2011). Understanding their complex interplay with the large-scale circulation (Marshall, 1984; Wunsch & Ferrari, 2004) is a major challenge in climate research, inevitably important to assess and predict climate change (Randall et al., 2007; Flato et al., 2013; Vallis, 2016). Eddies are capable of transferring energy across scales and are therefore a crucial element in the ocean's energy cycle (Rhines, 1979; Molemaker et al., 2005; Ferrari & Wunsch, 2009; Aiki et al., 2016). Finding a closure for eddies in ocean general circulation models is an active field of research (Eden, 2016; von Storch et al., 2012; Eden & Greatbatch, 2008). In addition to the energy cycle, eddies are also important for tracer transport and dominate the mixing and stirring of physical, chemical and biological water mass properties (Gent et al., 1995; Abernathey et al., 2010; Liu et al., 2012).

In the near future, state-of-the-art climate models will approach spatial resolutions at which the largest eddies can be resolved explicitly (Eyring et al., 2016). Despite the increasing performance of supercomputers, the most advanced Earth system models are not expected to fully resolve the mesoscale let alone the submesoscale (McWilliams, 2016) within the next decades. Western boundary currents (e.g. the Gulf Stream and Kuroshio) and their extension regions are an essential part in the wind-driven horizontal gyre circulation (Imawaki et al., 2013; Maximenko et al., 2013). These regions show an enhanced eddy activity on scales of several hundreds of kilometres down to the subme-

soscale (Ferrari & Wunsch, 2010). The need for more sophisticated turbulence
closures, realistically parameterizing the effect of meso- and submesoscale eddies
on the resolved flow, is hence clear.

Traditional approaches to eddy parameterization employ down-gradient fluxes
(Gent & McWilliams, 1990), ensuring numerical stability (Griffies, 2004), al-
though evidence exists that eddies also affect the mean circulation via up-
gradient momentum fluxes (Greatbatch et al., 2010; Wang et al., 2017). Some
approaches introduce stochasticity to account for sub-grid scale variability and
parameterizations are formulated as a function of the resolved flow and random
numbers, aiming to increase the number of variables that determine the future
evolution of the flow field (Palmer, 2001; Berloff, 2005; Jansen & Held, 2014;
Andrejczuk et al., 2016; Zanna et al., 2017). Physically motivated is the imple-
mentation of eddy viscosity as a diffusive turbulence closure to mimic the general
tendency of the eddy field to mix and hence smooth gradients (Smagorinsky,
1963; Leith, 1967; Redi, 1982; Griffies & Hallberg, 2000). Other approaches
aim to parameterize the advective effects of eddies in baroclinic instability and
mixed layer stratification (Gent & McWilliams, 1990; Fox-Kemper & Ferrari,
2008; Fox-Kemper et al., 2011; Brüggemann & Eden, 2014), but do not in-
clude considerations of the kinetic energy cycle. Generally speaking, there are
two main requirements that an eddy closure should satisfy in ocean circulation
models: (i) the physical parameterization of instabilities, their stirring and mix-
ing, and subsequent dissipation; and (ii) numerical stability through dissipation
of enstrophy at the grid scale. The viscosity in general circulation models is
usually tuned to satisfy (ii), whereby viscosity coefficients are several orders of
magnitude larger than would result from molecular considerations (Griffies &
Hallberg, 2000). This leads to a significant dissipation of energy in most ap-
proaches. We therefore believe successful parameterizations should aim to close
the energy cycle by reducing the effective viscosity that otherwise leads to a
spurious energy dissipation at the grid scale (Eden, 2016; Jansen & Held, 2014;
Arbic et al., 2007).

Eddy parameterizations that allow for upscale and downscale fluxes of en-

4

ergy are under investigation (e.g. Berloff (2005); Nadiga (2008); Eden (2010); Marshall et al. (2012); Porta Mana & Zanna (2014); Mak et al. (2016); Zanna et al. (2017)). A recently proposed approach (Jansen & Held, 2014; Jansen et al., 2015b) involves the combination of a hyperviscous closure in order to remove energy and enstrophy from the grid scale with a prognostic variable for the sub-grid eddy kinetic energy (EKE). The dissipated EKE is conserved and progressively re-injected into the resolved flow at larger scales via a deterministic term that is formulated as negative Laplacian viscosity. The effectively reduced dissipation allows for higher levels of EKE, thus hopefully improving the mean state and large-scale variability. The approach was shown to be successful in an idealised ocean model in a channel configuration (Jansen et al., 2015b). Here, we apply and extend the parameterization to a shallow water model driven by double gyre wind forcing with an idealized basin geometry and no-slip boundary conditions, and provide evidence for its general applicability.

This study is structured as follows. Section 2 briefly presents the shallow water model used throughout this study and its energetics. The formulation of sub-grid scale EKE and the resulting energy budget-based backscatter parameterization is introduced subsequently. In section 3.1 we discuss the model bias of the low resolution control run without parameterization with respect to the high resolution truth as reference. The impact of the energy budget-based backscatter parameterization on the low resolution model is analysed in section 3.2, and discussed in section 4. Finally, we summarise the results in section 5.

2. Methods

2.1. The shallow water model

The shallow water model (Gill, 1982; Vallis, 2006) of the prognostic variables velocity $\mathbf{u} = (u, v)$ and sea surface elevation η that is used in this study is

$$\frac{\partial \mathbf{u}}{\partial t} + (\mathbf{u} \cdot \nabla)\mathbf{u} + f\widehat{\mathbf{z}} \times \mathbf{u} = -g\nabla\eta + \mathbf{F} + \mathbf{B} + \mathbf{D} + \mathbf{\Xi} \qquad (1a)$$

$$\frac{\partial \eta}{\partial t} + \nabla \cdot (\mathbf{u}h) = 0. \qquad (1b)$$

5

We use a similar barotropic (gravity $g = 10$ ms^{-1}, density $\rho = 10^3$ kgm^{-3}) double gyre basin as in Cooper & Zanna (2015): To resemble a highly idealised North Atlantic, we use a square domain of size $L^2 = 3840$ km $\times$ 3840 km with Cartesian coordinates (x, y) centred at 30°N and a constant undisturbed

85 ocean depth of $H = 500$ m. The layer thickness is $h = \eta + H$. With the beta-plane approximation, the Coriolis parameter increases linearly from $f = 3.5 \times 10^{-5}$ s^{-1} at the southern boundary of the domain to $f = 1.1 \times 10^{-4}$ s^{-1} at the northern boundary. $\hat{\mathbf{z}}$ is a unit vector pointing in the upwards vertical direction. Boundary conditions are no-slip, as free-slip conditions were found

90 to lead to a highly unrealistic representation of the western boundary current. Steady and solely zonal double gyre wind forcing $\mathbf{F} = (F_x, 0)$

$$F_x = \frac{\tau}{\rho h}, \quad \tau = F_0 \left(\cos(2\pi y L^{-1} - \pi) + 2\sin(2\pi y L^{-1} - \pi) \right) \qquad (2)$$

with amplitude $F_0 = 0.12$ Pa is used (Fig. 1d). Model simulations start from rest ($\mathbf{u} = 0$) and the sea surface elevation is undisturbed ($\eta = 0$) in the initial conditions. Bottom friction $\mathbf{B}$ is represented as a quadratic drag $\mathbf{B} = -\frac{c_D}{h}|\mathbf{u}|\mathbf{u}$

95 with dimensionless drag coefficient $c_D = 10^{-5}$, which reduces energy primarily on large scales by approximately 30% compared to simulations without bottom friction. The drag is two orders of magnitude weaker than proposed by Arbic & Scott (2008) as the flow speed at the bottom of the ocean is much smaller than the barotropic flow speed simulated by the model. In practice, a weak

100 drag allows to maintain vigorous turbulence. Lateral mixing of momentum $\mathbf{D}$ is represented as a biharmonic version of the diffusion operator formulated by Shchepetkin & O'Brien (1996)

$$\mathbf{D} = -\nu_B h^{-1} \nabla \cdot (h \mathcal{S}(h^{-1} \nabla \cdot h \mathcal{S})), \quad \mathcal{S}(u, v) = \begin{pmatrix} u_x - v_y & v_x + u_y \\ v_x + u_y & -(u_x - v_y) \end{pmatrix} \qquad (3)$$

with a constant viscosity coefficient ν_B, that depends on the grid spacing Δx as $\nu_B = 540$ m^{2}s$^{-1} \frac{\Delta x^3}{30\text{km}}$. The resulting Munk boundary layer (Gill, 1982) is re-

105 solved with at least one grid cell for $\Delta x \leq 30$ km. The symmetric stress tensor $\mathcal{S}$ is once evaluated with (u, v) and once with $h^{-1} \nabla \cdot h \mathcal{S}(u, v)$ for biharmonic

6

diffusion. We call the biharmonic stress tensor $\mathcal{S}^* = \mathcal{S}(h^{-1}\nabla \cdot h\mathcal{S}(u,v))$. The term $\boldsymbol{\Xi}$ represents backscatter from unresolved scales and will be defined later. For the unparameterized control runs we set $\boldsymbol{\Xi} = 0$. The advection of momen-
₁₁₀ tum is split into a vorticity part and a gradient of kinetic energy, and we use the energy and enstrophy conserving scheme proposed by Arakawa & Lamb (1981) to discretise the former. Similar to the arguments of Jansen et al. (2015b), we favour this scheme as a sophisticated energy and enstrophy budget is central to the study.
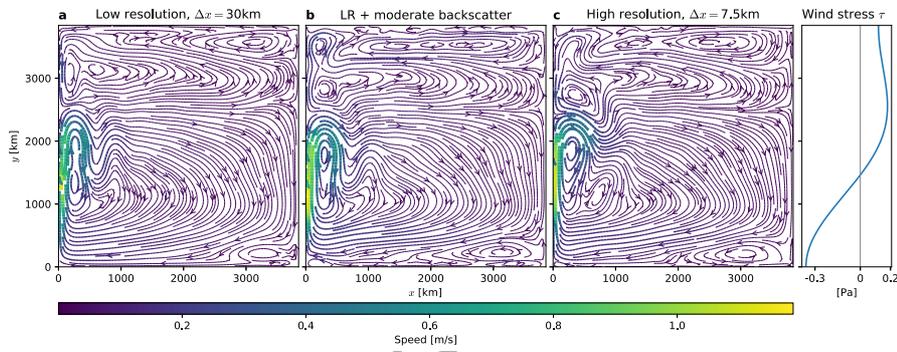
Figure 1: (a,b,c) Climatological mean circulation represented as stream lines calculated from (u,v). Colour and thickness of the stream lines are associated with speed. (d) Steady and solely zonal double gyre wind stress τ.

₁₁₅ Without backscatter, the energy budget of the shallow water equations is

$$\frac{\partial}{\partial t}\langle \tfrac{1}{2}\rho h|\mathbf{u}|^2 + \tfrac{1}{2}g\rho\eta^2\rangle = \langle u\tau\rangle - \langle \rho c_D|\mathbf{u}|^3\rangle - \langle \rho\nu_B h\nabla\mathbf{u}\cdot\mathcal{S}^*\rangle \qquad (4)$$

where the first term on the left-hand side represents kinetic energy (KE) and the second potential energy (PE). The brackets denote a horizontal domain-wide integral. These terms are further Reynolds-decomposed into mean and eddy contributions to kinetic and potential energy (MKE, EKE, MPE, EPE),
₁₂₀ respectively,

$$\begin{aligned}
\text{MKE} &= \tfrac{1}{2}\rho\overline{h}(\widehat{u}^2 + \widehat{v}^2), & \text{EKE} &= \tfrac{1}{2}\rho\overline{h(u''^2 + v''^2)}, \\
\text{MPE} &= \tfrac{1}{2}g\rho\overline{\eta}^2, & \text{EPE} &= \tfrac{1}{2}g\rho\overline{\eta'^2}.
\end{aligned} \qquad (5)$$

7
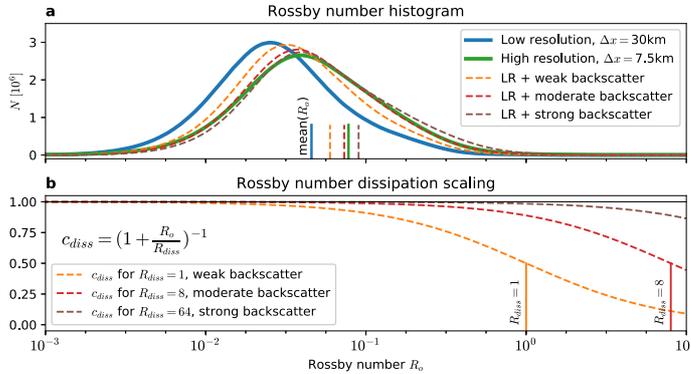
Figure 2: (a) Rossby number histogram for all grid points and time steps disregarding spin-up. The histogram from the high resolution run is scaled to match the histograms at low resolution. Time and spatial mean Rossby numbers are marked as vertical ticks for all model runs in corresponding line styles and colours. Bins are evenly spaced on a logarithmic axis. (b) Rossby number dissipation scaling c_{diss} for different backscatter strength controlled by R_{diss}.

The sea surface elevation is decomposed into a time mean and anomalies as $\eta = \overline{\eta} + \eta'$. Velocities are time averaged with thickness-weighting $\widehat{u} = \overline{hu}/\overline{h}$ and similarly for v (Aiki et al., 2016). The respective anomaly is $u'' = u - \widehat{u}$. In Eq. (4), the term $\langle u\tau \rangle$ represents power input due to wind forcing. The

₁₂₅ second term on the right-hand side denotes dissipation due to bottom friction and the third term on the right-hand side represents KE dissipation due to the biharmonic viscosity. Although harmonic diffusion is always down-gradient, biharmonic diffusion operators are not sign-definite and can also lead to power input (Griffies, 2004) but are mostly an energy sink, as will be discussed later.

₁₃₀ *2.2. Formulation of the energy budget-based backscatter parameterization*

Following the ideas of Eden & Greatbatch (2008) for a mesoscale eddy closure, which are further developed in Jansen & Held (2014) and Jansen et al. (2015a), we seek to find an energy equation for the unresolved scales applied to the shallow water equations. Similar to Jansen et al. (2015b) we comple-
₁₃₅ ment the shallow water equations with the following prognostic equation for the

8

vertically integrated sub-grid EKE, e:

$$\frac{\partial e}{\partial t} = -\dot{E}_{\text{diss}} + \dot{E}_{\text{back}} + \nu_e \nabla^2 e. \tag{6}$$

The energy dissipation from the resolved flow due to biharmonic diffusion is represented with $\dot{E}_{\text{diss}}$. Adding this term to the prognostic equation of sub-grid EKE is therefore a transfer of energy from the resolved to the unresolved flow.

The term $\dot{E}_{\text{back}}$ represents the tendency associated with the backscatter, hence the energy transfer from the sub-grid EKE budget back onto the resolved flow, which is realised with negative Laplacian viscosity. From the perspective of the sub-grid EKE, the first term on the right-hand side acts as a forcing, the second is a damping term, the third is a diffusion term. We set a constant diffusivity coefficient $\nu_e = 540\text{m}^2\text{s}^{-1}$ and $\nabla e = 0$ serves as boundary condition. As in Jansen et al. (2015b) we neglect any advection of sub-grid EKE with the mean flow due to a lack of an adequate theory that represents the combined effect of advection and wave propagation.

Omitting the constant density ρ, the EKE transfer to the unresolved flow associated with biharmonic dissipation follows from Eq. (4)

$$\dot{E}_{\text{diss}} = c_{\text{diss}}\nu_B h \nabla \mathbf{u} \cdot \mathcal{S}^* \tag{7}$$

This term is negative where the biharmonic diffusion removes energy from the resolved flow. In contrast to Jansen et al. (2015b) we introduce a spatially and temporally varying scaling for c_{diss}, which obeys $0 \leq c_{\text{diss}} \leq 1$, to allow only a fraction of the dissipated EKE to enter the sub-grid EKE budget. This is done for the following reasons:

(i) In the real ocean, the direction of energy cascades (upscale or downscale) depends on the local geostrophic balance and baroclinicity (Scott & Wang, 2005; Arbic et al., 2007; Capet et al., 2008; Ferrari & Wunsch, 2009; Molemaker et al., 2010; Brüggemann & Eden, 2015). A varying c_{diss} allows for an EKE transfer to the sub-grid EKE budget that is conditioned on properties of the locally resolved flow.

9

(ii) Having $c_{\text{diss}} < 1$ yields an energy sink for the resolved flow, as the fraction $1 - c_{\text{diss}}$ is not subject to the recycling process of the backscatter parameterization. This is desired for reasons of numerical stability: Choosing $c_{\text{diss}} = 1$, which corresponds to the original choice in Jansen et al. (2015b), may lead to an effective dissipation that is too weak, especially when other routes to dissipation are negligible.

The loss of energy via forward cascades arising in unbalanced flows is represented using

$$c_{\text{diss}} = \left(1 + \frac{R_o}{R_{\text{diss}}}\right)^{-1} \tag{8}$$

with the Rossby number $R_o = \frac{|D|}{f}$ estimated locally via the deformation rate $|D| = \sqrt{(u_x - v_y)^2 + (u_y + v_x)^2}$. Eq. (8) obeys the condition $0 \leq c_{\text{diss}} \leq 1$ for a positive non-dimensional constant R_{diss}, which controls the backscatter strength and remains subject to tuning. Having a deformation rate-based scaling of dissipation via c_{diss} means that regions of strong shear, especially boundary currents that are subject to no-slip boundary conditions, experience a stronger dissipation than elsewhere, in agreement with Zhai et al. (2010). This avoids re-injecting locally an excess amount of energy via the backscatter term where it may lead to spurious oscillations at the grid scale, which could in turn cause numerical instabilities. Physically speaking, we want to overcome the spurious energy dissipation at the grid scale for balanced flows ($R_o \ll 1$) but retain the dissipative character for unbalanced flows with large Rossby number (Rhines, 1979; Zhai et al., 2010; Molemaker et al., 2010; Nadiga, 2014). This is motivated by the fact that geostrophic turbulence at small Rossby numbers tends to undergo an upscale cascade of energy (Scott & Wang, 2005), whereas large Rossby numbers are indicative of a downscale cascade where energy should indeed be dissipated (Brüggemann & Eden, 2015; Molemaker et al., 2010; Ferrari & Wunsch, 2009). In that sense, we interpret R_{diss} as a cut-off Rossby number beyond which loss of balance can lead to a strong forward energy cascade (Fig. 2b)

The backscatter forcing term in the shallow water equations is formulated

10

similar to the biharmonic viscosity, but in the corresponding harmonic form with a negative viscosity coefficient to allow for an upscale transfer of energy.

$$\Xi = h^{-1}\nabla \cdot \nu_{\text{back}}h\mathcal{S}, \quad \nu_{\text{back}} = -c_{\text{back}}\Delta x\sqrt{\max(2\frac{e}{h}, 0)}. \tag{9}$$

Using a shallow water model, we consider the vertically integrated sub-grid EKE with units m^3s^{-2}, which alters the scaling for ν_{back} slightly through dividing by

195 h, in contrast to the original formulation in Jansen et al. (2015b), so that ν_{back} retains its physical units as m^2s^{-1}. c_{back} is an $\mathcal{O}(1)$ non-dimensional constant, which we set as originally proposed to be 0.4 and do not perform sensitivity experiments as the dependence on this parameter was previously shown to be weak. Eq. (6) can predict negative values of e, hence using the maximum

200 guarantees no backscatter in this case.

Similar to the derivation that led to Eq. (7), the backscatter term decreases the sub-grid EKE as

$$\dot{E}_{\text{back}} = \nu_{\text{back}}h\nabla\mathbf{u}\cdot\mathcal{S}. \tag{10}$$

and transfers that energy back to the resolved flow via negative viscosity. A list of all model runs used in this study is given in Table 1.

List of model runs	N	Δx [km]	ν_B [m^4s^{-1}]	R_{diss}	t_c
Low resolution (LR)	128^2	30	$4.86 \cdot 10^{11}$	-	1
High resolution (HR)	512^2	7.5	$7.59 \cdot 10^9$	-	50
LR + weak backscatter	128^2	30	$4.86 \cdot 10^{11}$	1	1.4
LR + moderate backscatter	128^2	30	$4.86 \cdot 10^{11}$	8	1.4
LR + strong backscatter	128^2	30	$4.86 \cdot 10^{11}$	64	1.4

Table 1: List of model runs used in this study. The total number of grid cells is denoted with N, the grid spacing with Δx. ν_B is the biharmonic viscosity coefficient. The tuning parameter for the backscatter strength is R_{diss}. The total cpu time t_c is given in relation to the computing time of the low resolution control run. Please note that the total cpu time is only roughly estimated and heavily dependent on the computing architecture.

11

Snapshots of relative vorticity
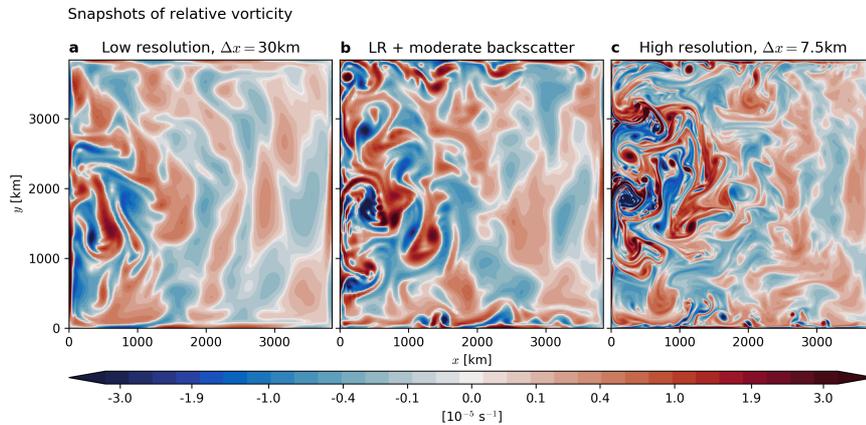
Figure 3: Snapshots of relative vorticity after 30 years of model integration. Positive vorticity is associated with anti-clockwise rotation and vice versa. Please note the non-linear colour map to highlight non-extreme structures.

3. Results

3.1. Comparing low and high resolution control runs

Looking at snapshots of relative vorticity provides insight into the dynamics simulated at different resolution (Fig. 3a and c). At high resolution, eddies of different sizes are apparent in most of the western part of the domain as well as in the proximity of the southern and northern boundaries. At low resolution, larger eddies are simulated where the boundary current leaves the western boundary but they do not propagate as far into the domain. Also, the proximity of the northern and the southern boundary are rather eddy-free. The circulation dynamics are mostly dominated by westward propagating Rossby waves in the eastern part of the domain and eddy-eddy interactions in the west (Greatbatch & Nadiga, 2000; Marshall, 1984). The double gyre circulation is not obvious from snapshots, but the climatological mean velocities (Fig. 1a and c) provide evidence for its existence. At low and high resolution a strong boundary current reaching speeds of about 1 ms^{-1} is simulated. The southern (northern) gyre is referred to as sub-tropical (sub-polar) gyre. The low resolution model shows weak additional gyres in the north-east and south-east corner, which are more

12
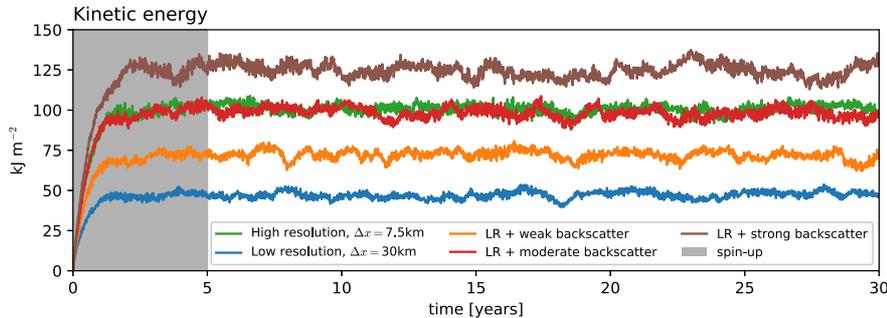
Figure 4: Spatially integrated kinetic energy for 30-year long integrations of model runs as described in Table 1. The spin-up phase of 5 years is omitted for all analyses. Kinetic energy is defined in Eq. (4).

extensive and carry more transport at high resolution. These counter-rotating gyres share similarities with those described by Greatbatch & Nadiga (2000) as potential vorticity gradients are flattened towards the boundary, but in a much weaker sense.

₂₂₅

Comparing the energy levels between the high and low resolution model, we conclude that the low resolution model lacks kinetic energy in the spatial and climatological mean by a factor of 2 to 2.5 (Fig. 4). This is mainly due to missing EKE at low resolution. The reservoir of EKE in the central western part of the domain, which is a factor of 2 larger at high resolution, dominates the energy budget (Fig. 5). The MKE is only large in the western boundary current and less dependent on resolution. This supports the notion that only the boundary current of the basin-wide circulation is a persistent strong current, whereas the instantaneous flow in other parts of the domain is dominated by eddies. Potential energy is one order of magnitude lower than kinetic energy, but similar conclusions hold concerning resolution-dependence (Fig. 5), as kinetic and potential energy are directly related in quasi-geostrophic flow (Vallis, 2006).

₂₃₀

₂₃₅

Although the biharmonic viscosity is known to remove energy at the grid scale (Griffies & Hallberg, 2000; Jansen & Held, 2014; Jansen et al., 2015b), it affects all spatial scales as seen in the EKE spectrum (Fig. 6). Most EKE is

₂₄₀

13
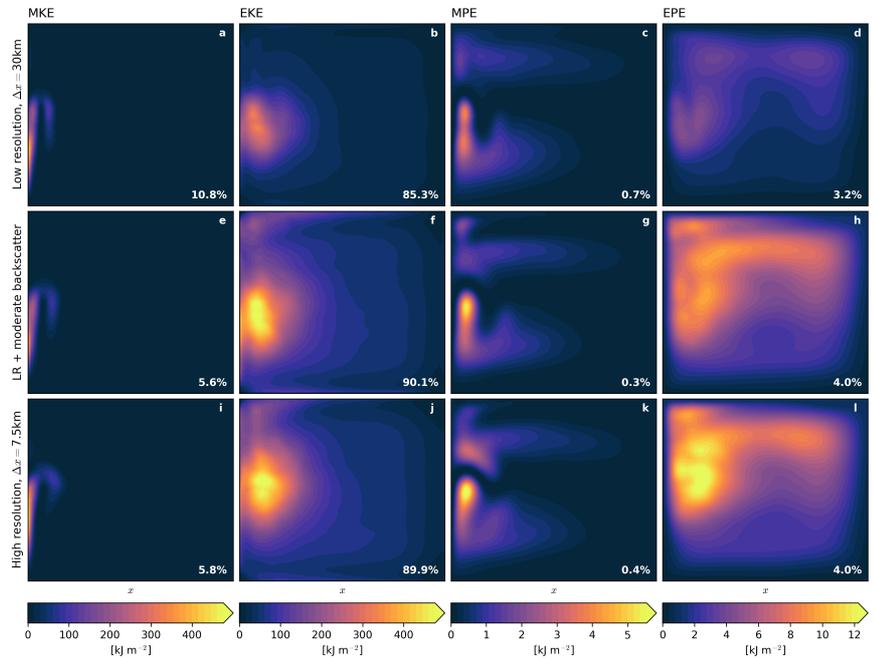
Figure 5: Climatological mean of mean kinetic energy (MKE), eddy kinetic energy (EKE), mean potential energy (MPE) and eddy potential energy (EPE). Percent value in the lower right corner of each sub-plot denote the relative contribution to the total energy defined as the sum of MKE, EKE, MPE and EPE.

concentrated on spatial scales near the Rossby deformation radius with a power law decrease close to K^{-3} (with K being the horizontal wavenumber) at smaller scales, pointing to a clearly developed turbulence cascade over a wide range of scales. The EKE is reduced at low resolution by approximately the same factor across length scales of 200km to 2000km compared to high resolution.

In order to understand the differences in eddy energy that come with different resolution, the sources and sinks to the energy budget are analysed. Wind forcing is found to be locally either an energy source or an energy sink, which depends on the direction of the zonal flow compared to the direction of the wind forcing (Fig. 7a and g), but less so on the resolution. In a spatially integrated sense, wind forcing is the only energy source to the shallow water system in the

14
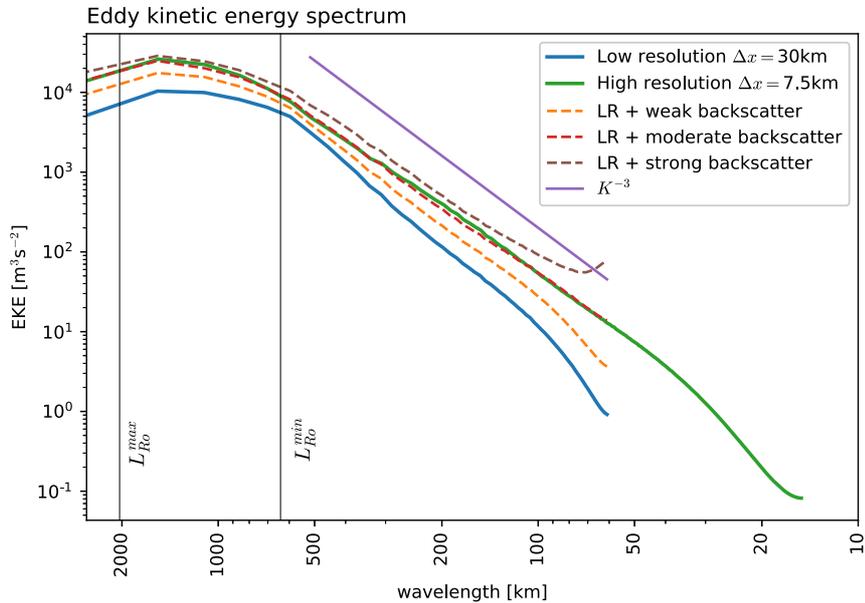
Figure 6: Eddy kinetic energy spectrum. The spectral energy is logarithmically plotted against horizontal wavenumber K but for readability relabelled with the corresponding wavelength. A theoretical spectrum of K^{-3} is given for comparison. The barotropic Rossby radii of deformation for the southern (northern) boundary of the domain $L_{R_o}^{\max}$ ($L_{R_o}^{\min}$) are given for orientation.

physical settings of this study, and approximately independent of the resolution. Bottom friction removes energy primarily from the western boundary current and its extension, where flow speeds are fastest (Fig. 7b and h). The pattern
255 therefore resembles that of MKE (Fig. 5a and i). The power due to the viscosity term reveals an energy sink in the eddy-dominated central western part of the domain, which is strong at low resolution but much weaker at high resolution (Fig. 7c and i). The viscosity in connection with no-slip boundary conditions also removes a substantial part of the energy from the boundary. Due to a not
260 sign-definite biharmonic viscosity operator, some of the energy that is removed directly at the boundary is partly re-injected a few grid cells further inward. At high resolution 64% of dissipation is through bottom friction, and only 36% due

15
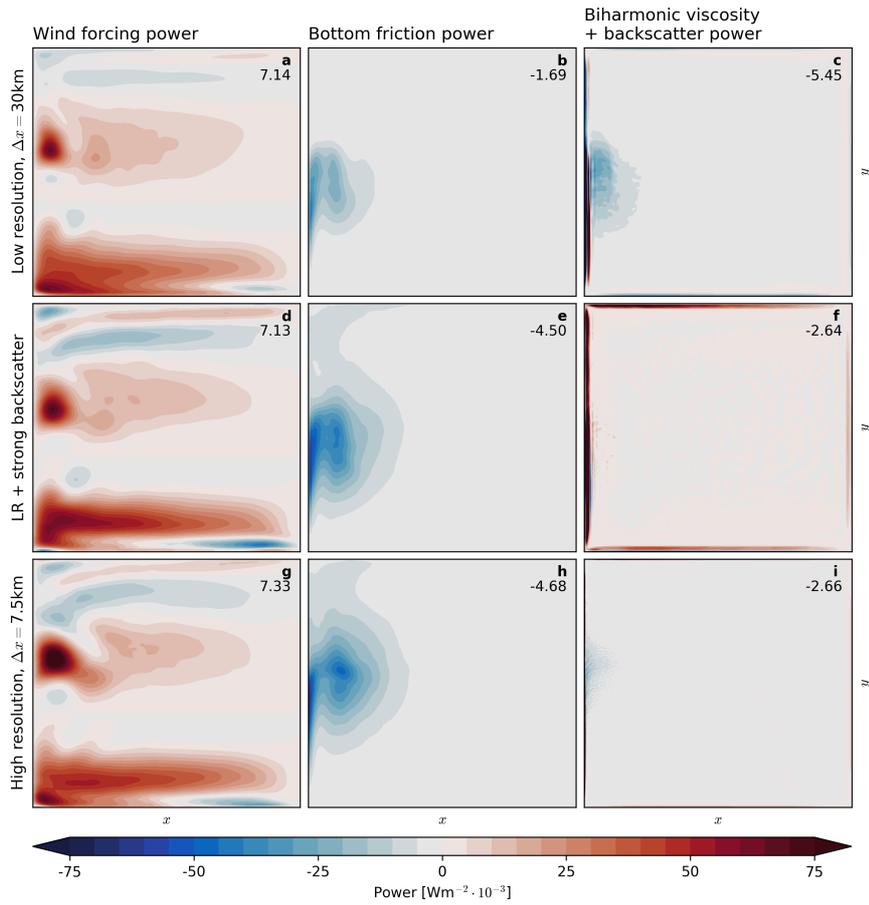
Figure 7: Climatological mean of energy sources and sinks due to wind forcing, bottom friction, viscosity and backscatter. Positive (negative) values indicate an energy source (sink). Backscatter power is zero for low and high resolution control run. In (c,f,i) the most extreme values occur at the boundary and are up to one order of magnitude beyond the color scale. The numbers in the top right of each sub-plot denote a domain-wide average in units of 10^{-3} Wm^{-2}.

16

to viscosity. This ratio is clearly different at low resolution, where viscosity is responsible for 76% of dissipation.

₂₆₅ Distributions of Rossby numbers reveal that the low resolution model is not able to reproduce the turbulent nature of the simulated flow at high resolution as Rossby numbers are in general lower by a factor of 2 (Fig. 2a). Based on this and the other diagnostics shown (Fig. 1, 4-7), we conclude that a low resolution model differs statistically from its high resolution version that is taken as refer-

₂₇₀ ence. For lower resolution, it is necessary to increase the viscosity coefficient in the model (Table 1) to prevent numerical instabilities. This pushes the dissipative scales into the eddy scales, leading to a depression of eddy activity (Nadiga & Straub, 2010). The unrealistically high viscosity therefore affects the physical regime of the flow, measured here in terms of the Rossby number. Decreased

₂₇₅ eddy kinetic and potential energy follow, affecting the mean circulation and the variability of the flow.

3.2. Energy-budget based backscatter

The spurious viscous energy dissipation in the low resolution model can be counteracted using the backscatter approach. In the original formulation by

₂₈₀ Jansen et al. (2015b) all dissipated EKE is transferred to the sub-grid EKE budget (i.e. $c_{\mathrm{diss}} = 1$ in Eq. 7). The case of $c_{\mathrm{diss}} = 1$ is not going to be discussed here, as significant spurious energy tendencies occur due to excessive numerical noise at the boundaries. Instead, our strong backscatter simulation, which closely resembles this limit, uses a dissipation weakly dependent on the

₂₈₅ Rossby number, with $R_{\mathrm{diss}} = 64$ (see Eq. 8).

Having no-slip boundary conditions, a large amount of energy is dissipated via viscosity due to strong shear flows at the boundary (Fig. 7c and i), especially at low resolution. Consequently, most sub-grid EKE is concentrated in the western boundary region in the climatological mean (Fig. 8c). Additionally,

₂₉₀ the central western interior shows increased sub-grid EKE levels as following from a pronounced EKE dissipation via viscosity in the highly turbulent region between the sub-tropical and sub-polar gyre (Fig. 7c). The explicit diffusion

17

of sub-grid EKE in its prognostic equation has a negligible effect as the time scale for the grid-scale diffusion is on the order of 20 days for $\nu_e = 540$ m^{2}s^{-1},

²⁹⁵ whereas the backscatter time scale, defined as the residence time of sub-grid EKE, is on the order of hours to a day. The negligible role of sub-grid diffusion is also supported by an experiment with an increased sub-grid EKE diffusion ($\nu_e = 5400$ m^{2}s^{-1}), which reproduces virtually the same results. Solely negative values of sub-grid EKE are absent in the climatological mean (Fig. 8) due to

³⁰⁰ the increased diffusion, but with a negligible impact on the resolved flow.
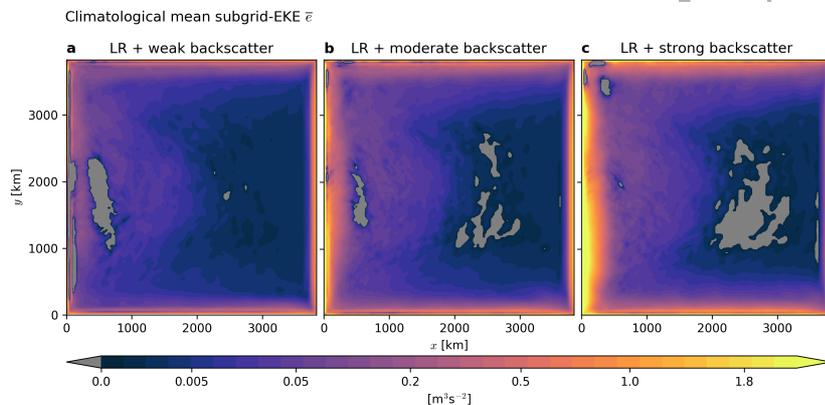
Figure 8: Climatological mean of the sub-grid EKE variable e for different backscatter strength. Please note the non-linear colour map to highlight lower values. Grey areas have a negative sub-grid EKE as the biharmonic dissipation is not sign-definite but are not accounted for in the backscatter term (Eq. 9).

The source of energy to the resolved flow via the backscatter parameterization increases with the local level of sub-grid EKE (Eq. 9). It follows therefore that the backscatter parameterization leads to a particularly strong forcing near the boundaries. In the strong backscatter case, the EKE spectrum shows

³⁰⁵ a strong energy increase at the grid scale, indicative of numerical noise (Fig. 6). Snapshots, especially of relative vorticity, reveal that these numerical oscillations occur in the vicinity of boundary currents due to weak dissipation (not shown). Furthermore, in the strong backscatter case energy levels exceed those of the high resolution run on all scales (Fig. 4 and 6), and the histogram of

18

Rossby numbers (Fig. 2a) reveals that high Rossby number flow is too prevalent, whereas low Rossby number flow is too rare compared to the high resolution run. Hence, it would be desirable to decrease the strength of the backscatter parameterization, especially near the western boundary.

The only considered parameter to tune the flow-regime dependent backscatter strength is the positive scalar R_{diss}. We find for $R_{\mathrm{diss}} < 1$, the effect of the backscatter to be negligible, such that the low resolution run with backscatter converges towards its unparameterized control run. A moderate backscatter parameterization ($R_{\mathrm{diss}} = 8$) is tuned so as to match the kinetic energy level of the high resolution run (Fig. 4). Remarkably, this also coincides with a corrected EKE spectrum (Fig. 6).

The climatological mean of EKE (Fig. 5) in the moderate backscatter case is virtually identical to its reference at high resolution. Also EPE is considerably improved and relative contributions of the different energy reservoirs to the total energy are in good agreement with those of the high resolution run (Fig. 5). The energy cycle is corrected, as bottom friction accounts for most dissipation (Fig. 7e). Combining the energy sources and sinks of the biharmonic viscosity and the backscatter term reveals the net effect of the sub-grid parameterization (Fig. 7f), which is in overall agreement with viscous dissipation at high resolution (Fig. 7i). Notice that the patterns in Figs. 7f and 7i are not expected to be identical, as the two represent energy exchange between the resolved and sub-grid flow at different cut-off scales. Importantly, however, the total sub-grid energy dissipation rate, which represents the magnitude of the forward energy cascade, is similar in the two simulations.

Increased EKE levels coincide with a higher eddy activity, especially in regions where eddies are absent without backscatter parameterization (Fig. 3). This has a positive effect on the climatological mean circulation as the eddy-driven circulations along the northern and southern boundaries are in much better agreement with those simulated at high resolution (Fig. 1). Furthermore, a moderate strength backscatter parameterization yields Rossby numbers distributions that closely resemble those simulated at high resolution (Fig. 2a).

19

4. Discussion

While the original Jansen et al. (2015b) parameterization is shown to lead to an excess of EKE at the grid scale in the vicinity of strong boundary currents with no-slip boundary conditions, the generalisation presented in this study

345 overcomes this limitation by introducing a Rossby number-based dissipation scaling that yields an energy sink for geostrophically unbalanced flow (Molemaker et al., 2010; Ferrari & Wunsch, 2009; Rhines, 1979). We are thus able to eliminate the numerical distortions at the western boundary that would otherwise limit the practicality of the backscatter parameterization. The eddy-mean

350 flow interaction in a low resolution model is shown to be enhanced, enabling the model to simulate an improved climatological mean state, that presumably results from increased levels of EKE and EPE due to a more sophisticated simulation of the energy cycle. We want to emphasise that the tuning of the backscatter strength is solely motivated by matching reference kinetic energy

355 levels. Remarkably, main aspects of the mean circulation are improved without tuning towards an optimised mean state.

For the sake of simplicity, computational power and given the importance of horizontal scales, we have focussed here on the two dimensional shallow water equations, which we find adequate to simulate eddy-mean flow interactions as

360 a predominant process in the spectrum of geostrophic turbulence in the global oceans. An idealised ocean basin is considered, which represents a sub-tropical to sub-polar ocean basin as a rectangular domain without realistic coast lines or bottom topography. Nevertheless, we suggest that the simplified geometry does not influence the major results of this study because processes of large-

365 scale geostrophic turbulence occur similarly in all ocean basins with variable coastlines and bottom topography (Chelton et al., 2011; von Storch et al., 2012). The shallow water model considered does, however, have several shortcomings that limit the comparability to the real ocean. Many of the processes that lead to a forward cascade of energy in the real ocean (such as interactions with

370 bottom topography and internal waves) are missing in our model (e.g. Gertz

20

& Straub (2009)). Furthermore, only the vertically integrated sub-grid EKE is considered. It remains an open question how to parameterize vertical fluxes of sub-grid EKE in a more advanced three dimensional ocean general circulation model permitting baroclinic instability.

₃₇₅ For simplicity, we used a constant viscosity coefficient for the biharmonic lateral mixing of momentum. More sophisticated approaches exist (Smagorinsky, 1963; Leith, 1967; Griffies & Hallberg, 2000), promoting the use of a flow- and scale-aware non-linear viscosity coefficient in order to remove enstrophy from the grid-scale and satisfy numerical stability. However, none of these approaches
₃₈₀ simultaneously dissipate enstrophy without also dissipating excessive amounts of energy on the grid scale, the primary motivation for using the backscatter approach. A Smagorinsky-like formulation of the biharmonic viscosity was successfully combined with the backscatter parameterization (Jansen et al., 2015b). As the constant viscosity coefficient used here provides comparable improve-
₃₈₅ ments, we believe that the energy-budget based backscatter parameterization is applicable to various forms of diffusion operators as long as viscosity is in a biharmonic form (or of even higher order) and backscatter is formulated with a harmonic operator.

5. Summary and conclusion

₃₉₀ An energy budget-based backscatter parameterization for the unresolved scales in a shallow water model driven by double gyre wind forcing is presented. The parameterization is an extension of the original approach by Jansen et al. (2015b) using a biharmonic viscosity in combination with an additional deterministic forcing term, formulated as negative Laplacian viscosity, to represent
₃₉₅ backscatter of energy from unresolved scales (Jansen & Held, 2014). The kinetic energy that is removed from the resolved flow enters the sub-grid EKE budget, which is introduced as a prognostic variable. Based on local levels of sub-grid EKE, the previously dissipated energy is re-injected at larger spatial scales via the backscatter term, corresponding to an artificial upscale transfer

21

of energy and hence a closure for the energy cycle. Simultaneously, enstrophy is dissipated at the grid scale, ensuring numerical stability. A newly formulated Rossby number-based dissipation scaling allows for a route to energy dissipation for geostrophically unbalanced flow as supported by theory and observations.

The backscatter parameterization presented in this study is shown to substantially improve the model, effectively improving the simulation equivalent to about a factor of two to four increase in resolution at negligible additional computational cost. While the implementation of an energy budget-based backscatter parameterization in a global climate model may not be straightforward, we provide evidence for its potential to substantially improve the models currently used for weather and climate prediction. We therefore highly promote further research on energy budget-based backscatter methods.

Finally, we want to emphasise the importance of closing the energy cycle in an ocean circulation model (Eden, 2016) for successful climate simulations and a better prediction of climate change. Understanding the routes to dissipation in geophysical turbulence is a major challenge in theory and observations and is an essential basis for sophisticated parameterizations of unresolved scales. The energy budget-based backscatter approach provides the potential to implement realistic routes to dissipation in an ocean circulation model, which provides a cornerstone for improved climate predictions.

Conflict of interest

The authors declare that they have no conflict of interest.

Author contributions

MK, MFJ and RJG designed the study. MK wrote the numerical model, conducted experiments, performed the analysis and wrote the manuscript. MC contributed to the development of the numerical model. All authors contributed in discussion of the results and the manuscript.

Acknowledgements

Supplementary materials

Data relevant to this study is available in Klöwer (2018a). A more detailed description of the shallow water model used, its discretisation as well as model, analysis and plotting scripts can be found in Klöwer (2018b).

Abernathey, R., Marshall, J., Mazloff, M., & Shuckburgh, E. (2010). Enhancement of Mesoscale Eddy Stirring at Steering Levels in the Southern Ocean. *Journal of Physical Oceanography*, *40*, 170–184. doi:10.1175/2009JPO4201.1.

Aiki, H., Zhai, X., & Greatbatch, R. J. (2016). Energetics of the Global Ocean: the Role of Mesoscale Eddies. *Indo-Pacific Climate Variability and Predictability*, (pp. 109–134).

Andrejczuk, M., Cooper, F. C., Juricke, S., Palmer, T. N., Weisheimer, A., & Zanna, L. (2016). Oceanic Stochastic Parameterizations in a Seasonal Forecast System. *Monthly Weather Review*, *144*, 1867–1875. doi:10.1175/MWR-D-15-0245.1. arXiv:1506.09181.

Arakawa, A., & Lamb, V. R. (1981). A Potential Enstrophy and Energy Conserving Scheme for the Shallow Water Equations. doi:10.1175/1520-0493(1981)109<0018:APEAEC>2.0.CO;2.

Arbic, B. K., Flierl, G. R., & Scott, R. B. (2007). Cascade Inequalities for ForcedDissipated Geostrophic Turbulence. *Journal of Physical Oceanography*, *37*, 1470–1487. doi:10.1175/JPO3067.1.

Arbic, B. K., & Scott, R. B. (2008). On Quadratic Bottom Drag, Geostrophic Turbulence, and Oceanic Mesoscale Eddies. *Journal of Physical Oceanography*, *38*, 84–103. doi:10.1175/2007JPO3653.1.

Berloff, P. S. (2005). Random-forcing model of the mesoscale oceanic eddies. *Journal of Fluid Mechanics*, *529*, 71–95. doi:10.1017/S0022112005003393.

Brüggemann, N., & Eden, C. (2014). Evaluating Different Parameterizations for Mixed Layer Eddy Fluxes induced by Baroclinic Instability. *Journal of Physical Oceanography*, *44*, 2524–2546. doi:10.1175/JPO-D-13-0235.1.

Brüggemann, N., & Eden, C. (2015). Routes to Dissipation under Different Dynamical Conditions. *Journal of Physical Oceanography*, *45*, 2149–2168. doi:10.1175/JPO-D-14-0205.1.

Capet, X., McWilliams, J. C., Molemaker, M. J., & Shchepetkin, A. F. (2008). Mesoscale to Submesoscale Transition in the California Current System. Part I: Flow Structure, Eddy Flux, and Observational Tests. *Journal of Physical Oceanography*, *38*, 29–43. doi:10.1175/2007JPO3671.1.

Chelton, D. B., Schlax, M. G., & Samelson, R. M. (2011). Global observations of nonlinear mesoscale eddies. *Progress in Oceanography*, *91*, 167–216. doi:10.1016/j.pocean.2011.01.002.

Cooper, F. C., & Zanna, L. (2015). Optimisation of an idealised ocean model, stochastic parameterisation of sub-grid eddies. *Ocean Modelling*, *88*, 38–53. doi:10.1016/j.ocemod.2014.12.014.

Eden, C. (2010). Parameterising meso-scale eddy momentum fluxes based on potential vorticity mixing and a gauge term. *Ocean Modelling*, *32*, 58–71. doi:10.1016/j.ocemod.2009.10.008.

24

Eden, C. (2016). Closing the energy cycle in an ocean model. *Ocean Modelling*, *101*, 30–42. doi:10.1016/j.ocemod.2016.02.005.

Eden, C., & Greatbatch, R. J. (2008). Towards a mesoscale eddy closure. *Ocean Modelling*, *20*, 223–239. doi:10.1016/j.ocemod.2007.09.002.

Eyring, V., Bony, S., Meehl, G. A., Senior, C. A., Stevens, B., Stouffer, R. J., & Taylor, K. E. (2016). Overview of the Coupled Model Intercomparison Project Phase 6 (CMIP6) experimental design and organization. *Geoscientific Model Development*, *9*, 1937–1958. doi:10.5194/gmd-9-1937-2016.

Ferrari, R., & Wunsch, C. (2009). Ocean Circulation Kinetic Energy: Reservoirs, Sources, and Sinks. *Annual Review of Fluid Mechanics*, *41*, 253–282. doi:10.1146/annurev.fluid.40.111406.102139.

Ferrari, R., & Wunsch, C. (2010). The distribution of eddy kinetic and potential energies in the global ocean. *Tellus, Series A: Dynamic Meteorology and Oceanography*, *62*, 92–108. doi:10.1111/j.1600-0870.2009.00432.x.

Flato, G., Marotzke, J., Abiodun, B., Braconnot, P., Chou, S., Collins, W., Cox, P., Driouech, F., Emori, S., Eyring, V., Forest, C., Gleckler, P., Guilyardi, E., Jakob, C., Kattsov, V., Reason, C., & Rummukainen, M. (2013). Evaluation of Climate Models. *Climate Change 2013: The Physical Science Basis. Contribution of Working Group I to the Fifth Assessment Report of the Intergovernmental Panel on Climate Change*, (pp. 741–866). doi:10.1017/CBO9781107415324. arXiv:arXiv:1011.1669v3.

Fox-Kemper, B., Danabasoglu, G., Ferrari, R., Griffies, S. M., Hallberg, R. W., Holland, M. M., Maltrud, M. E., Peacock, S., & Samuels, B. L. (2011). Parameterization of mixed layer eddies. III: Implementation and impact in global ocean climate simulations. *Ocean Modelling*, *39*, 61–78. doi:10.1016/j.ocemod.2010.09.002.

Fox-Kemper, B., & Ferrari, R. (2008). Parameterization of Mixed Layer Eddies.

Part II: Prognosis and Impact. *Journal of Physical Oceanography*, *38*, 1166–1179. doi:10.1175/2007JPO3788.1.

Gent, P. R., & McWilliams, J. C. (1990). Isopycnal Mixing in Ocean Circulation Models. doi:10.1175/1520-0485(1990)020<0150.

510   Gent, P. R., Willebrand, J., McDougall, T. J., & McWilliams, J. C. (1995). Parameterizing Eddy-Induced Tracer Transports in Ocean Circulation Models. *Journal of Physical Oceanography*, *25*, 463–474. doi:10.1175/1520-0485(1995)025<0463.

Gertz, A., & Straub, D. N. (2009). Near-Inertial Oscillations and the Damping
515   of Midlatitude Gyres: A Modeling Study. *Journal of Physical Oceanography*, *39*, 2338–2350. doi:10.1175/2009JPO4058.1.

Gill, A. E. (1982). *Atmosphere-Ocean Dynamics*. Academic Press.

Greatbatch, R. J., & Nadiga, B. T. (2000). Four-Gyre Circulation in a Barotropic Model with Double-Gyre Wind Forcing. *J. Phys. Oceanogr*, *30*,
520   1461–1471. doi:10.1175/1520-0485(2000)030<146.

Greatbatch, R. J., Zhai, X., Claus, M., Czeschel, L., & Rath, W. (2010). Transport driven by eddy momentum fluxes in the Gulf Stream Extension region. *Geophysical Research Letters*, *37*, 1–6. doi:10.1029/2010GL045473.

Griffies, S. M. (2004). Fundamentals of ocean climate models. *Princeton Uni-*
525   *versity Press*, (p. 518 pp).

Griffies, S. M., & Hallberg, R. W. (2000). Biharmonic Friction with a Smagorinsky-Like Viscosity for Use in Large-Scale Eddy-Permitting Ocean Models. *Monthly Weather Review*, *128*, 2935–2946. doi:10.1175/1520-0493(2000)128<2935.

530   Imawaki, S., Bower, A. S., Beal, L., & Qiu, B. (2013). *Ocean Circulation and Climate - A 21st Century Perspective* volume 103. doi:10.1016/B978-0-12-391851-2.00013-1.

Jansen, M. F., Adcroft, A. J., Hallberg, R., & Held, I. M. (2015a). Parameterization of eddy fluxes based on a mesoscale energy budget. *Ocean Modelling*, *92*, 28–41. doi:10.1016/j.ocemod.2015.05.007.

Jansen, M. F., & Held, I. M. (2014). Parameterizing subgrid-scale eddy effects using energetically consistent backscatter. *Ocean Modelling*, *80*, 36–48. doi:10.1016/j.ocemod.2014.06.002.

Jansen, M. F., Held, I. M., Adcroft, A., & Hallberg, R. (2015b). Energy budget-based backscatter in an eddy permitting primitive equation model. *Ocean Modelling*, *94*, 15–26. doi:10.1016/j.ocemod.2015.07.015.

Klöwer, M. (2018a). Data from shallow water model: Control simulations and backscatter experiments. URL: https://data.geomar.de/thredds/catalog/open_access/kloewer_et_al_2018_om/catalog.html.

Klöwer, M. (2018b). milankl/swm: Shallow water model. doi:10.5281/zenodo.1403130.

Leith, C. E. (1967). Diffusion Approximation to Inertial Energy Transfer in Isotropic Turbulence. *Physics of Fluids*, *10*, 1409. doi:10.1063/1.1762300.

Liu, C., Köhl, A., & Stammer, D. (2012). Adjoint-Based Estimation of Eddy-Induced Tracer Mixing Parameters in the Global Ocean. *Journal of Physical Oceanography*, *42*, 1186–1206. doi:10.1175/JPO-D-11-0162.1.

Mak, J., Maddison, J. R., & Marshall, D. P. (2016). A new gauge-invariant method for diagnosing eddy diffusivities. *Ocean Modelling*, *104*, 252–268. doi:10.1016/j.ocemod.2016.06.006.

Marshall, D. P., Maddison, J. R., & Berloff, P. S. (2012). A Framework for Parameterizing Eddy Potential Vorticity Fluxes. *Journal of Physical Oceanography*, *42*, 539–557. doi:10.1175/JPO-D-11-048.1.

Marshall, J. C. (1984). Eddy-mean flow interaction in a barotropic ocean model. doi:10.1002/qj.49711046502.

Maximenko, N., Lumpkin, R., & Centurioni, L. (2013). *Ocean Circulation and Climate - A 21st Century Perspective* volume 103. doi:10.1016/B978-0-12-391851-2.00012-X.

McWilliams, J. C. (2016). Submesoscale currents in the ocean. *Proceedings of the Royal Society of London A*, *472*, 1–32. doi:10.1098/rspa.2016.0117.

Molemaker, M. J., McWilliams, J. C., & Capet, X. (2010). Balanced and unbalanced routes to dissipation in an equilibrated Eady flow. *Journal of Fluid Mechanics*, *654*, 35–63. doi:10.1017/S0022112009993272.

Molemaker, M. J., McWilliams, J. C., & Yavneh, I. (2005). Baroclinic Instability and Loss of Balance. *Journal of Physical Oceanography*, *35*, 1505–1517. doi:10.1175/JPO2770.1.

Nadiga, B. T. (2008). Orientation of eddy fluxes in geostrophic turbulence. *Philosophical Transactions of the Royal Society A: Mathematical, Physical and Engineering Sciences*, *366*, 2489–2508. doi:10.1098/rsta.2008.0058.

Nadiga, B. T. (2014). Nonlinear evolution of a baroclinic wave and imbalanced dissipation. *Journal of Fluid Mechanics*, *756*, 965–1006. doi:10.1017/jfm.2014.464.

Nadiga, B. T., & Straub, D. N. (2010). Alternating zonal jets and energy fluxes in barotropic wind-driven gyres. *Ocean Modelling*, *33*, 257–269. doi:10.1016/j.ocemod.2010.02.007.

Palmer, T. N. (2001). A nonlinear dynamical perspective on model error: A proposal for non-local stochastic-dynamic parametrization in weather and climate prediction models. *Quarterly Journal of the Royal Meteorological Society*, *127*, 279–304. doi:10.1002/qj.49712757202.

Porta Mana, P. G. L., & Zanna, L. (2014). Toward a stochastic parameterization of ocean mesoscale eddies. *Ocean Modelling*, *79*, 1–20. doi:10.1016/j.ocemod.2014.04.002.

28

Randall, D., Wood, R., Bony, S., Colman, R., Fichefet, T., Fyfe, J., Kattsov, V., Pitman, A., Shukla, J., Srinivasan, J., Stouffer, R., Sumi, A., & Taylor, K. (2007). Climate models and their evaluation. *Climate Change 2007:*

⁵⁹⁰ *The Phisical Science Basis. Contribution of Working Group I to the Fourth Assessment Report on the Intergovernmental Panel on Climate Change*, . doi:10.1016/j.cub.2007.06.045.

Redi, M. H. (1982). Oceanic Isopycnal Mixing by Coordinate Rotation. doi:10.1175/1520-0485(1982)012<1154.

⁵⁹⁵ Rhines, P. B. (1979). Geostrophic Turbulence. *Annual Review of Fluid Mechanics*, *11*, 401–441. doi:10.1175/1520-0469(1971)028<1087.

Scott, R. B., & Wang, F. (2005). Direct Evidence of an Oceanic Inverse Kinetic Energy Cascade from Satellite Altimetry. *Journal of Physical Oceanography*, *35*, 1650–1666. doi:10.1175/JPO2771.1.

⁶⁰⁰ Shchepetkin, A. F., & O'Brien, J. J. (1996). A Physically Consistent Formulation of Lateral Friction in Shallow-Water Equation Ocean Models. doi:10.1175/1520-0493(1996)124<1285.

Smagorinsky, J. (1963). General Circulation Experiments With the Primitive Equations. *Monthly Weather Review*, *91*, 99–164. doi:10.1175/

⁶⁰⁵ 1520-0493(1963)091<0099.

von Storch, J.-S., Eden, C., Fast, I., Haak, H., Hernández-Deckers, D., Maier-Reimer, E., Marotzke, J., & Stammer, D. (2012). An Estimate of the Lorenz Energy Cycle for the World Ocean Based on the STORM/NCEP Simulation. *Journal of Physical Oceanography*, *42*, 2185–2205. doi:10.1175/

⁶¹⁰ JPO-D-12-079.1.

Vallis, G. K. (2006). *Atmospheric and Ocean Fluid Dynamics*. Cambridge University Press.

Vallis, G. K. (2016). Geophysical fluid dynamics: whence, whither and why? *Proceedings of the Royal Society A: Mathematical, Physical and Engineering Science*, *472*, 20160140. doi:10.1098/rspa.2016.0140.

Wang, Y., Claus, M., Greatbatch, R. J., & Sheng, J. (2017). Decomposition of the Mean Barotropic Transport in a High-Resolution Model of the North Atlantic Ocean. *Geophysical Research Letters*, (pp. 537–546). doi:10.1002/2017GL074825.

Wunsch, C., & Ferrari, R. (2004). Vertical Mixing, Energy, and the General Circulation of the Oceans. *Annual Review of Fluid Mechanics*, *36*, 281–314. doi:10.1146/annurev.fluid.36.050802.122121.

Zanna, L., Porta Mana, P., Anstey, J., David, T., & Bolton, T. (2017). Scale-aware deterministic and stochastic parametrizations of eddy-mean flow interaction. *Ocean Modelling*, *111*, 66–80. doi:10.1016/j.ocemod.2017.01.004.

Zhai, X., Johnson, H. L., & Marshall, D. P. (2010). Significant sink of ocean-eddy energy near western boundaries. *Nature Geoscience*, *3*, 608–612. doi:10.1038/ngeo943.

30